ChemMedChem

Research Article
doi.org/10.1002/cmdc.202200508

Chemistry Europe
European Chemical Societies Publishing

www.chemmedchem.org

A Neutral and Stable Macrocyclic Mn(II) Complex for MRI Tumor Visualization

Loredana Leone,[a] Annasofia Anemone,[b] Antonella Carella,[c] Elena Botto,[c] Dario Livio Longo,*[c] and Lorenzo Tei*[a]

A stable and inert amphiphilic Mn(II) complex based on a bisamide derivative of 1,4-DO2A (DO2A = tetraazacyclododecane-1,4-diacetic acid) was synthesized and its ^{1}H NMR relaxometric behavior was investigated as a function of the magnetic field strength, pH and temperature. The interaction with human serum albumin (HSA) was also studied via relaxometry showing a good relaxivity enhancement at low field (at 1T and 298 K the relaxivity increases from 4.5 $mM^{-1}s^{-1}$ of the Mn(II)-complex to 14.0 $mM^{-1}s^{-1}$ of the complex-HSA supramolecular adduct). In vivo biodistribution and MRI studies highlighted a rapid and mixed renal/liver elimination without spleen accumulation from healthy mice and good contrast enhancing properties in a breast tumor murine model. A comparison with a clinically approved Gd(III) agent (GdBOPTA, Multihance®) underlined that the proposed Mn(II) contrast agent gave comparable tumor contrast enhancement up to 3 hours post-injection.

Introduction

The research on contrast agents (CAs) for magnetic resonance imaging (MRI) has recently increasingly directed the efforts towards paramagnetic Mn(II) and Fe(III) complexes as alternatives to the well-established Gd(III)-based agents (GBCAs) regularly used in the clinical setting.[1–5] The reason relies on the association of some linear GBCA with a potentially fatal disease called nephrogenic systemic fibrosis (NSF) caused by the release of toxic free Gd ions in patients suffering from chronic kidney disease.[6] Moreover, the recent discovery of the presence of small amounts of Gd in the tissues of patients exposed to multiple MRI scans, although without any evidence that this is associated with clinical harm,[7] has further boosted the search for alternative CAs.

Compared to GBCAs, Mn(II) CAs has the major advantage of having a better safety profile, since manganese is an essential element, and the organs of living systems possess efficient mechanisms to manage the in vivo levels of this ion.[2,3] Despite the biogenic nature of Mn(II), the relatively high paramagnetic metal concentrations typically used in MRI (ca. 0.1–0.2 mmol kg^{-1}) require the use of thermodynamically stable and kinetically inert complexes. On the other hand, the Mn-chelate should possess at least one water molecule coordinated to the central metal ion (hydration number, $q \geq 1$) to allow positive contrast on T_1-weighted MR images.

Among the recently studied Mn-chelates, only a few are sufficiently inert to be used in vivo. Within the group of open-chain ligands, the Mn-complexes with the rigid (1,2-cyclohexandiamino)tetraacetic acid (CDTA) and its derivatives (i.e., PyC3A, Scheme 1) display the best features.[8,9] The acyclic $[Mn(PyC3A)(H_2O)]^-$ chelate was also tested in vivo providing excellent MR contrast, similar to that of GdDTPA (Magnevist®), and showing an elimination from the body via renal and hepatic pathways.[10,11] Considering the macrocyclic ligands, Mn(II) complexes with PC2A and derivatives (PC2A = tetraazabicyclo [9.3.1]pentadeca-1(15),11,13-triene-3,9-diacetic acid, Scheme 1) have been reported to possess excellent thermodynamic stability and kinetic inertness for further in vivo studies.[12,13] Moreover, the six donor atoms of the ligands provide enough space for the coordination of a water molecule to the metal centre allowing to obtain good relaxivity values. Thus, a PC2A chelator bearing a biphenyl moiety for Human Serum Albumin (HSA) binding permitted the visualization of the murine brain vascular system by using low CA doses.[14] Another interesting, rigid and preorganized, recently reported Mn(II) complex (*i.e.* Mn-bispidine) that shows a not very high thermodynamic stability but a strong resistance to acid catalyzed dissociation and transmetalation, might be an excellent option as a Mn-based MRI contrast agent.[15]

In case of 1,4,7,10-tetraazacyclododecane (cyclen) derivatives, our group has recently shown that 1,4-DO2A (Scheme 1) forms a Mn(II) complex with a good compromise between stability, inertness and relaxivity.[16] On the other hand, the Mn(1,7-DO2A) regioisomer displays similarly high stability and inertness, but no coordinated water molecule and, therefore,

[a] Dr. L. Leone, Prof. L. Tei
Department Science and Technological Innovation
University of Piemonte Orientale
Viale Teresa Michel 11, 15121 Alessandria (Italy)
E-mail: lorenzo.tei@uniupo.it
[b] Dr. A. Anemone
Department of Molecular Biotechnology and Health Sciences
University of Torino
Via Nizza, 52, 10126 Torino (Italy)
[c] Dr. A. Carella, Dr. E. Botto, Prof. D. L. Longo
Institute of Biostructures and Bioimaging (IBB)
National Research Council of Italy (CNR)
Via Nizza, 52, 10126 Torino (Italy)
E-mail: dariolivio.longo@cnr.it

Supporting information for this article is available on the WWW under https://doi.org/10.1002/cmdc.202200508

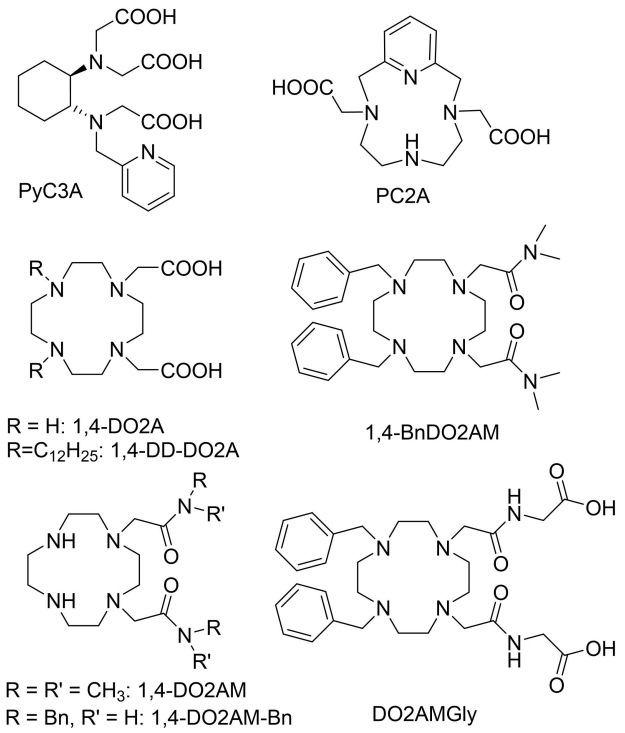

Scheme 1. Ligands discussed in the text.

low relaxivity.[17] The further modification of 1,4-DO2A including long aliphatic chains on the 7,10 positions of cyclen allowed to obtain amphiphilic Mn-complexes used to form supramolecular adducts with HSA and lipidic nanoparticles such as micelles and liposomes with high relaxivities and very interesting contrast enhancing properties.[18,19] Then, the substitution of the acetate with *N*,*N*-dimethylacetamide pendant arms (1,4-DO2AM) resulted in a Mn(II) chelate with a 20% increase of the relaxivity and an improvement of the kinetic inertness that reached a half-life of 556 h at pH 7.4.[20] Finally, the attachment of hydrophobic moieties such as benzyl groups on the secondary amines at the 7,10 positions of the macrocycle or on the amides to obtain 1,4-BnDO2AM and 1,4-DO2AM–Bn, respectively (Scheme 1), allowed the noncovalent binding to macromolecules such as HSA and thus a quite remarkable relaxivity enhancement.[21] In particular, Mn(1,4-BnDO2AM) showed a better thermodynamic stability ($\log K_{MnL} = 11.54$) and kinetic inertness ($t_{1/2} = 136$ h at pH 7.4) with respect to Mn(1,4-DO2AM–Bn). In addition, the interaction with HSA is stronger when the benzyl groups are attached to the macrocycle, although the relaxivity of the Mn-complex-HSA adduct is slightly lower.

Thus, in this work, we modified the structure of the ligand 1,4-BnDO2AM by adding an acetic group on the amides in 1,4 positions in order to obtain a neutral complex (MnDO2AMGly, Scheme 1), since excessively charged complexes are known to be susceptible to reduced stability, increased cellular internalization and nonspecific uptake and elimination by the reticuloendothelial system in organs such as the liver and spleen.[22,23] Moreover, serum albumin binding promotes, in addition to the higher relaxivity enhancement at low magnetic field strength, increased capability to assess fenestrated vessels in tumor regions in comparison to smaller molecular weight contrast agents.[24] Therefore, angiographic probes are still considered important for assessing microvascularization in tumors.[14,26–28]

Here we show the synthesis of MnDO2AMGly, its relaxometric characterization, including the analysis of the interaction with HSA and the ^{1}H NMR relaxometric study on the MnDO2AMGly-HSA adduct, the *in vivo* biodistribution and MR contrast enhancement properties in a breast tumor murine model.

Results and Discussion

Synthesis. The DO2AMGly ligand was synthesized, as shown in Scheme 2, by alkylation of 1,4-dibenzyl-cyclen with *N*-(2-Bromoacetyl)ethyl glycinate in the presence of Cs_2CO_3 as base followed by hydrolysis of the ethyl esters with LiOH. 1,4-dibenzyl-cyclen and N-(2-Bromoacetyl)ethyl glycinate were synthesized according to previously published procedures.[21,29] The final ligand was purified by semi-preparative HPLC and characterized by ^{1}H and ^{13}C NMR and ESI MS. The Mn(II) complex was synthesized by stirring an equimolar aqueous solution of ligand and manganese nitrate at pH 6.5.

^{1}H relaxometric study. The efficiency of a CA is described by its relaxivity (r_1), defined as the increase of the longitudinal water proton relaxation rate induced by 1 mM concentration of the paramagnetic ion. The r_1 value recorded at pH 7.4 (298 K, 20 MHz) for MnDO2AMGly is 4.6 $mM^{-1}s^{-1}$ (Table 1), 21% and 84% higher than those reported for Mn(1,4-BnDO2AM) and Mn(1,4-DO2AM) complexes, respectively, mainly due to the larger molecular mass.

The proton Nuclear Magnetic Relaxation Dispersion (^{1}H NMRD) profiles of aqueous solutions of MnDO2AMGly (Figure 1) were recorded at 298 and 310 K in the range of magnetic field strengths 2.3×10^{-4} to 3.0 T, which corresponds to proton Larmor frequencies 0.01–128 MHz. The NMRD profiles reproduce the typical shape of low molecular weight complexes in the fast water exchange regime, whose relaxivity is mostly dominated by rotational dynamics. In addition, the lower r_1 values at 310 K over the entire range of investigated proton Larmor frequencies with respect to those measured at 298 K

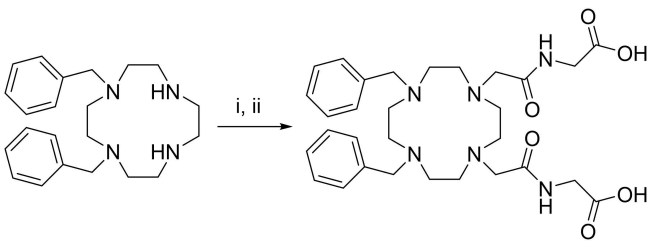

Scheme 2. Synthesis of DO2AMGly: i) *N*-(2-bromoacetyl) ethyl glycinate, Cs_2CO_3, DMF, 90 °C,24 h; ii) LiOH (0.5 M), MeOH 2 h, 50 °C.

Table 1. Relaxometric parameters for MnDO2AMGly and the supramolecular adduct MnDO2AMGly-HSA obtained from the analysis of ^{1}H NMRD data and compared to other relevant Mn(II)-complexes and HSA-adducts.[a]

	DO2AMGly	1,4-BnDO2AM[b]	1,4-DO2AM[c]	DO2AMGly-HSA	1,4-DD-DO2A-HSA[d]
r_1 at 25/37 °C, 20 MHz/mM^{-1} s^{-1}	4.6/3.4	3.8/2.8	2.5/2.0	14.7[e]	29.5[e]
$k_{ex}^{298}/10^7$ s^{-1}	16.4 ± 0.6	25.3	11.5	16.4[f]	34
$\Delta H^{\neq}$ kJ mol^{-1}	19.7 ± 1.2	14.4	39.8	–	–
τ_R^{298}/ps	115 ± 1	96	53	4×10^4	4×10^4
$^{298}\tau_{RL}$/ps	–	–	–	196 ± 15	629
S^2	–	–	–	0.12 ± 0.01	0.57
τ_v^{298}/ps	26.7 ± 1.5	13	5.5	47.5 ± 2.1	18
$\Delta^2/10^{19}$ s^{-2}	7.0 ± 0.4	20	51	2.2 ± 0.2	1.4
q^{298}	1	1	0.87	1	0.87
$A_O/\hbar/10^6$ rad s^{-1}	−33.0 ± 0.4	−31.0	−39.0	–	–
$n{\cdot}K_A$	–	–	–	(3.0 ± 0.2) × 10^3	2.3×10^4

[a] The following parameters were fixed to appropriate values during the fitting procedure: the hydration number q; the distance between Mn^{2+} and the protons of the bound water molecule, r, was set to 2.83 Å; the distance of closest approach, a, of the outer sphere water molecules to Mn^{2+} was set to 3.6 Å; the relative diffusion coefficient D^{298} was set to 2.24×10^{-5} cm^2 s^{-1}. The activation energies of D, E_D, of τ_R, E_R, and of τ_V, E_V, were set to at the values found for Mn(1,4-DO2A): 17.3, 19.1 and 1 kJ mol^{-1}, respectively; [b] Ref. [21]; [c] Ref. [20]; [d] Ref. [18].; [e] $r_1{}^b$ at 20 MHz and 298 K; [f] Fixed to the value obtained for MnDO2AMGly.

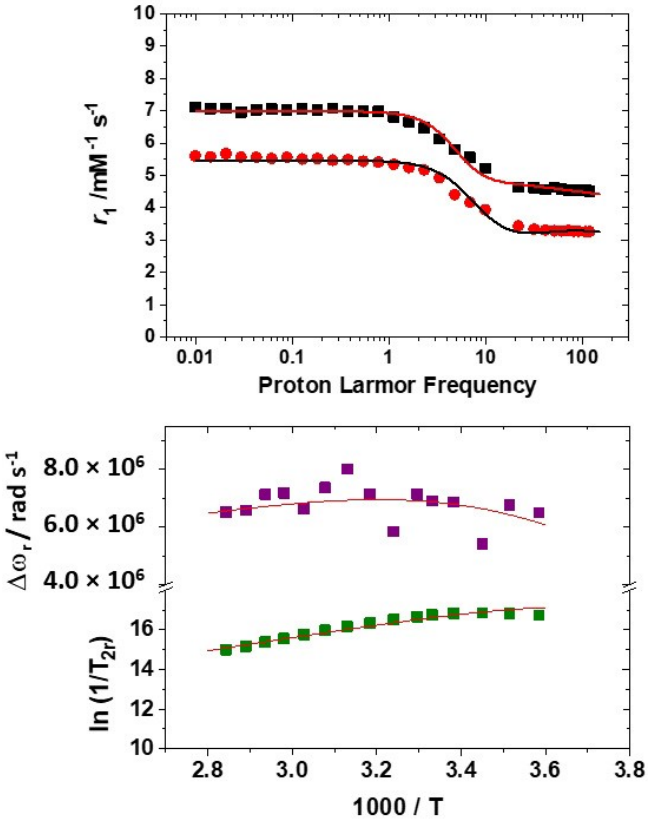

Figure 1. Top: ^{1}H NMRD profiles of MnDO2AMGly recorded at 298 K (black symbols) and 310 K (red symbols) and pH 7; bottom: reduced transverse ^{17}O NMR relaxation rates and chemical shifts versus reciprocal temperature measured for a 4 mM aqueous solution of MnDO2AMGly at 11.74 T and pH 7. The solid lines represent the best fitting results of the experimental data points with the parameters shown in Table 1.

indicates that r_1 is not limited by the water exchange rate but rather by the fast rotational motion of the complex.

In addition, to obtain detailed information on the water exchange parameters, the ^{17}O NMR reduced transverse relaxation rates ($1/T_{2r}$) and chemical shifts ($\Delta\omega_r$) of MnDO2AMGly were measured as a function of temperature (Figure 1). The complex shows an increase of the $1/T_{2r}$ value with decreasing temperature over the full temperature range, which is typical of systems under the fast exchange regime.

The simultaneous fitting of the ^{1}H NMRD and ^{17}O NMR data according to the established theory of paramagnetic relaxation[30] afforded the structural and dynamic molecular parameters shown in Table 1, compared to the parameters reported previously for related Mn(II) complexes. Some of the parameters were fixed during the analysis: the distance of closest approach for the outer-sphere contribution a_{MnH} at 3.6 Å; the distance between the Mn(II) ion and the proton nuclei of the coordinated water molecules (r_{MnH}) fixed at 2.83 Å; the diffusion coefficient, D^{298}, and its activation energy, E_D, were fixed to common values. Considering that MnDO2AMGly differs from the previously reported $[Mn(1,4\text{-BnDO2AM})]^{2+}$ only for the presence of acetylglycinate pendants in place of the acetate and that the Mn(II) coordination sphere remains unchanged, we took into account the number of inner sphere water molecules ($q=1$), reported previously.[20] The fit yielded a $k_{ex}=(16.4\pm0.6)\times10^6$ and $\Delta H^{\neq}=19.7\pm1.2$ kJ mol^{-1} in line with the values reported for the structurally analogue $[Mn(1,4\text{-BnDO2AM})]^{2+}$, albeit with a slightly slower exchange rate. Also the ^{17}O hyperfine coupling constants ($A_O/\hbar$) is in the range typically observed for small Mn(II) complexes. Furthermore, the rotational correlation time is slightly longer by ca. 20% than that reported for $[Mn(1,4\text{-BnDO2AM})]^{2+}$, in agreement with the higher molecular weight and the electron relaxation parameters, τ_V and Δ^2 agree to those obtained for other macrocyclic MnDO2A-like complexes.[16,20,21]

The presence of hydrophobic benzyl groups in the structure of MnDO2AMGly allows the binding of the complex to human serum albumin, the most abundant of the serum proteins. The binding interaction was investigated using the well-established proton relaxation enhancement (PRE) technique. This method consists in measuring the increase of the water proton longitudinal relaxation rate (R_1) of a diluted aqueous solution of the Mn-complex as a function of increasing concentration of

the protein (in the present case at 20 MHz and 298 K, Figure 2a). R_1 is enhanced by the increase of the fraction of bound complex, characterized by a longer τ_R. The fitting of the experimental data provides the values of the thermodynamic association constant, K_A, the number of the equivalent and independent binding sites, n, and the relaxivity of the resulting paramagnetic adduct r_1^{bound}. All the data were fitted to 1:1 binding isotherm even though the presence of multiple affinity sites on HSA cannot be excluded for this type of complexes (Table 1). In comparison to the analogous [Mn(1,4-BnDO2AM)]$^{2+}$,[20] the K_A for MnDO2AMGly is only slightly higher whereas the r_1^b is 25% lower, possibly due to the charge neutrality of MnDO2AMGly that reduces the interaction with the protein. The ^{1}H NMRD profile of the supramolecular adducts was recorded at neutral pH and 298 K under conditions ensuring that more than 98% of the chelate was bound to the protein (Figure 2).

The high field region of the profile (>1 T) was fitted to the SBM theory including the Lipari–Szabo approach for the description of the rotational dynamics.[31] This model considers a local rotation of the complex superimposed on the global reorientation of the supramolecular adduct. These two types of motion are characterized by different correlation times: τ_{RL} and τ_{RG}, respectively, related by the parameter S^2, which takes values between 0 (completely independent motions) and 1 (entirely correlated motions). A four-parameter (Δ^2, τ_V, τ_{RL} and S^2) least-squares fit of the data was performed and the best-fit parameters are listed in Table 1 and compared with the supramolecular system obtained by interacting the amphiphilic Mn(1,4-DD-DO2A) complex with HSA.[17] In this last system the interaction of the two dodecyl chains with HSA is stronger resulting in higher r_1^b and S^2 values with respect to the MnDO2AMGly-HSA adduct.

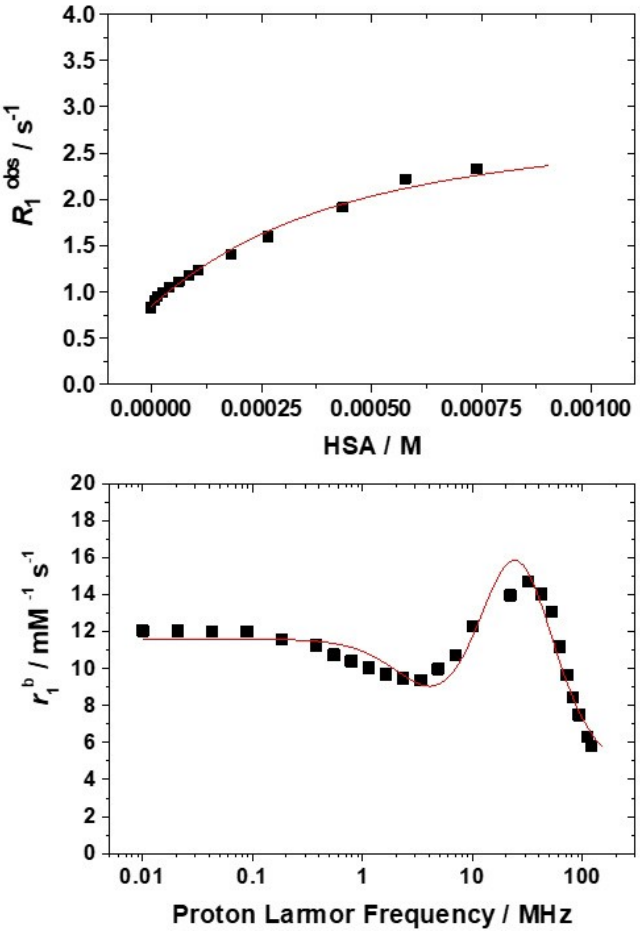

Figure 2. Top: changes in the observed longitudinal relaxation rates of water protons observed upon the addition of HSA to solutions of MnDO2AMGly (0.17 mM). The solid lines represent the least-squares fits of the data according to a 1:1 binding isotherm; bottom: ^{1}H NMRD profile at 298 K of MnDO2AMGly-HSA adduct. The solid line represents the best fitting results of the experimental data points with the parameters shown in Table 1.

Finally, although the parent [Mn(1,4-BnDO2AM)]$^{2+}$ complex showed a high thermodynamic stability and kinetic inertness, a stability test in physiological conditions *in vitro* was carried out. In fact, in case of a Mn(II)-complex insufficiently stable, plasma proteins could potentially initiate a transmetalation process and thus a release and binding of free Mn(II) to HSA. This binding would result in a strong increase in relaxivity, since the Mn(HSA) adduct presents a r_1 of 97.2 mM^{-1} s^{-1} at 20 MHz and 298 K.[32] Therefore, mixing a kinetically labile and thermodynamically unstable chelate with a Seronorm solution is expected to induce dissociation of the chelate, resulting in a great increase in the relaxation rate of the sample. In case of MnDO2AMGly, the relaxation rate of a solution of the complex in Seronorm remains constant for at least 50 h (Figure S1), indicating negligible dissociation of the complex, as expected due to the high kinetic inertness measured for the parent complex [Mn-(1,4-BnDO2AM)]$^{2+}$.[21]

***In vitro* and *in vivo* studies**. *In vitro* tissue culture experiments were used for pilot toxicity studies. The MnDO2AMGly complex was tested with J774 macrophage cells at increasing concentrations into the culture media and allowed to incubate for 24 h. The viability assay (Figure 3) indicated no statistically significant decrease in cell viability even at concentrations up to 0.1 mM, which translates in potential clinical application.

Upon intravenous administration of MnDO2AMGly longitudinal evolution of T_1-weighted MR images were recorded,

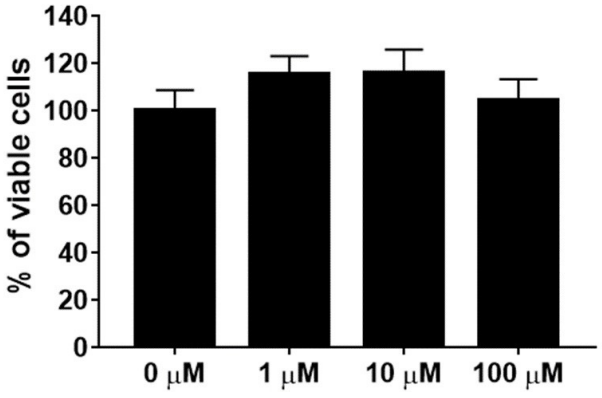

Figure 3. J774 macrophage cells incubated with different concentrations of MnDO2AMGly for 24 h, and percentage of viable cells using the standard MTT assay.

showing a rapid and mixed renal and liver elimination without spleen accumulation on healthy mice (Figure 4).

T_1-weighted MR images were used to calculate contrast enhancements at 5, 10, 15, 30 min and at 1, 2, 4 and 24 h upon *i.v.* administrations, with almost complete clearance 1 day after the injection. Signal enhancements peaked in the kidneys at 5 min after the injection and quickly decreased, suggesting urinary excretion.

A low signal enhancement was observed in the liver that remained constant up to 4 hours post injection. On the other hand, the signal in the heart is already reduced 5 min after injection, suggesting a rapid washout, whereas the time course of the signal in the gallbladder showed a marked enhancement with time (Figures S5 and S6). Overall, these results demonstrate that the elimination occurred through both the renal and hepatobiliary routes, as observed for other Mn-based agents.[33,34]

Contrast enhancement capabilities were also evaluated in female mice bearing HER/2+ TS/A breast tumors (that show well vascularized tumors)[35,36] with a 1T MRI preclinical scanner to exploit the higher relaxivity shown by paramagnetic complexes upon serum albumin binding at low magnetic field strength.[24,25] In addition, owing to the weak binding to serum albumin of MnDO2AMGly, we compared its contrast efficiency with that of GdBOPTA (MultiHance®), a commercial Gd-complex with weak plasma protein binding, serving as a control contrast agent, instead of comparing it with an extracellular fluid Gd-based agent.

MnDO2AMGly provided strong contrast enhancement of subcutaneous breast tumor lesions comparable to that observed upon GdBOPTA administration at the same dose in the tail vein of mice (Figure 5). At 2 min post-injection, GdBOPTA provided higher contrast enhancement than the Mn(II)-complex ($p < 0.001$), but for all the following time points the contrast enhancements remained comparable up to 3 hours post-injection. Both MnDO2AMGly and GdBOPTA showed higher contrast enhancements than in respective control muscle regions in the same mice at all time points. The observed intra-variability between both tumors for each mouse was quite low (Figure S7). Although several factors can contribute to different contrast enhancements between the two investigated agents upon administration, including differences in protein binding affinity, elimination rate and routes, contrast efficiency (relaxivity) and molecular size, the slightly higher enhancement observed for GdBOTPA at earlier time points could be explained by the higher relaxivity of this agent when bound to the serum albumin ($36\ mM^{-1}s^{-1}$ vs $15\ mM^{-1}s^{-1}$ for GdBOTPA and MnDO2AMGly, respectively, at 1T).[37]

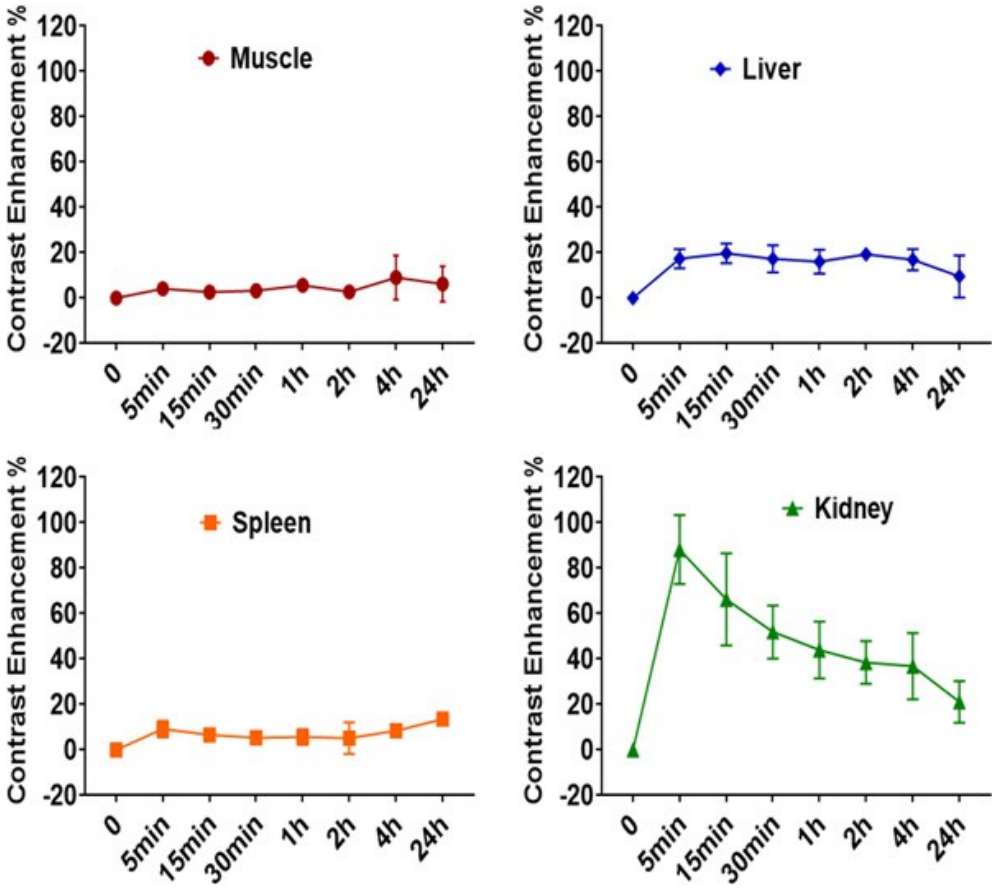

Figure 4. Signal enhancements time curves recorded before and up to 24 h after the intravenous injection of 0.03 mmol/kg MnDO2AMGly in the muscle, liver, spleen and kidneys of healthy mice.

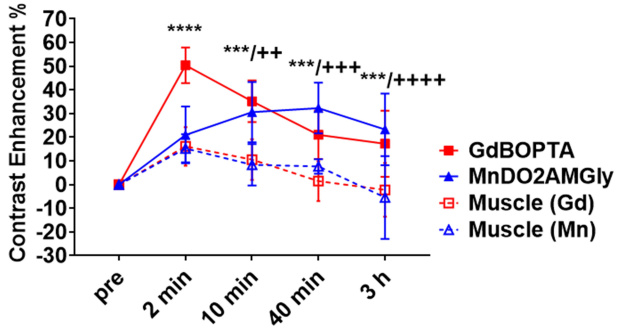

Figure 5. Contrast enhancements (CE%) measured in breast tumor bearing mice and in control muscle regions of the same mice after intravenous injection of Multihance® or of MnDO2AMGly at the same dose of 0.1 mmol/kg. (***$P<0.01$, ****$P<0.0001$ for GdBOPTA CE% in tumor vs muscle regions in the same mice at the same time points post-injection; $^{++}P<0.05$, $^{+++}P<0.001$ and $^{++++}P<0.0001$ for MnDO2AMGly CE% in tumor vs muscle regions in the same mice at the same time points post-injection).

Figure 6 shows representative T_1-weighted images before and at several time points after injection of 0.1 mmol Gd/kg dose of GdBOPTA and before and after an equal dose of MnDO2AMGly.

Conclusion

A new Mn(II) complex based on the 1,4-disubstituted tetraazamacrocycle cyclen bearing two acetylglycinate and two benzyl pendants was synthesized and characterized by ^{1}H NMR relaxometry. The presence of two benzyl groups in the positions 7, 10 allowed a good interaction with HSA and a 3-fold increase of the relaxivity in serum at 1T. The favorable relaxometric performance of this Mn(II)-complex encouraged the *in vitro* toxicity study on cells and the *in vivo* investigation on healthy and breast tumor bearing mice. No toxicity and a rapid and mixed renal and liver elimination without spleen accumulation was achieved in healthy mice, whereas a strong MRI signal enhancement (ca. 30%) on subcutaneous breast tumor lesions was observed after *i.v.* injection of MnDO2AMGly. The comparison with a clinically approved MRI agent showed that the contrast enhancement is comparable (except in the first two minutes after injection) and persistent up to 3 hours post-injection. This work is a further evidence that Mn(II) complexes can have interesting MRI applications as possible substitute of GBCAs.

Experimental Section

All chemicals were purchased from Sigma-Aldrich or Alfa Aesar unless otherwise stated and were used without further purification. 1,4-dibenzyl-1,4,7,10-tetraazacyclododecane and ethyl (2-bromoacetyl)glycinate were synthetized as reported elsewhere.[21,28] The ^{1}H and ^{13}C NMR spectra were recorded using a Bruker Advance III 500 MHz (11.4 T) spectrometer equipped with 5 mm PABBO probes and BVT-3000 temperature control unit. Chemical shifts are reported relative to TMS and were referenced using the residual

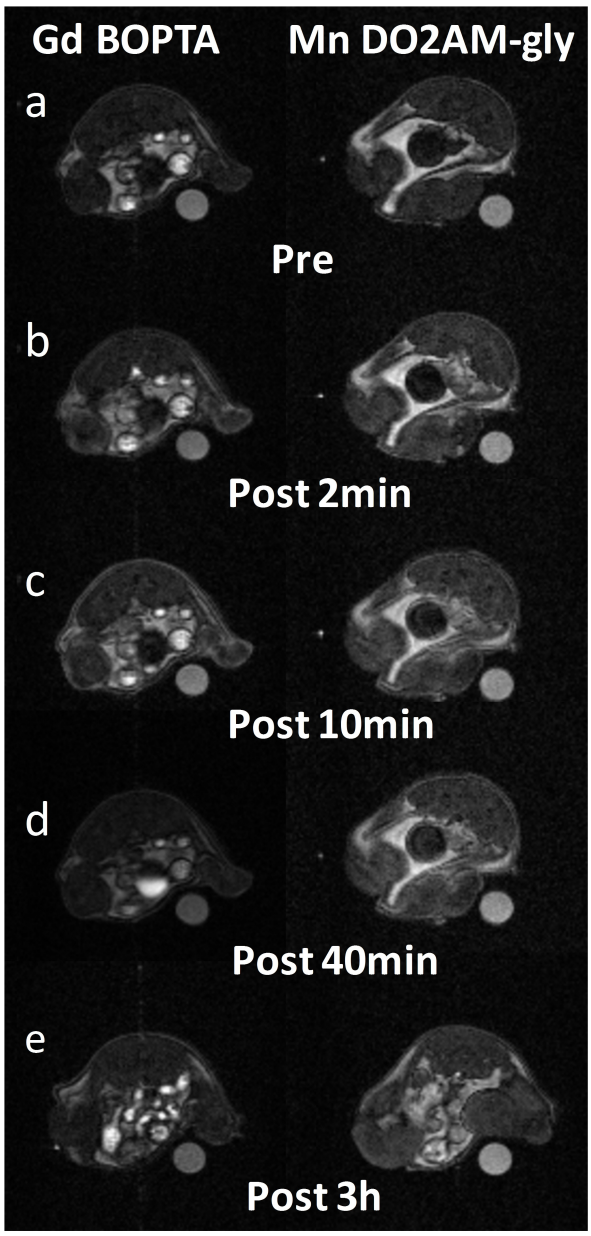

Figure 6. Representative contrast-enhanced MRI of a breast tumor murine model using GdBOPTA (left) and MnDO2AMGly (right). Axial MR images of the tumor before and after injection of 0.1 mmol /kg of Gd or Mn complex at several time points: pre (a), and post 2 min (b), 10 min (c), 40 min (d) and 3 h (e).

proton solvent resonances. HPLC analyses and mass spectra were performed on a Waters HPLC-MS system equipped with a Waters 1525 binary pumps. Analytical measurements were carried out on a Waters XBridge-Phenyl (5 µm 4.6×150 mm). (Method A): A = H_2O/0.1% TFA; B = MeOH; 1 mL/min flow; 0–2 min = 99% A; 2–15 min = from 99% A to 100% B; 15–19 min = 100% B. Semi-preparative purification were performed on a Waters XBridge-Phenyl Prep OBD (5 µm, 19x100 mm) (5 µm 19x100 mm) using the following method: (Method B): A = H_2O/0.1% TFA; B = MeOH; 20 mL/min flow; 0–3 min = 99% A; 3–7 min = from 99% A to 100% B; 7–8 min = 100% B. Electrospray ionization mass spectra (ESI MS) were recorded using a SQD 3100 Mass Detector (Waters), operating in positive or

negative ion mode, with 1% v/v formic acid in methanol as the carrier solvent.

Synthesis of diethyl 2,2′-((2,2′-(7,10-dibenzyl-1,4,7,10-tetraazacyclododecane-1,4-diyl)bis(carboxymethylglycinate). 1,4-dibenzyl-1,4,7,10-tetraazacyclododecane (0.25 g, 0.71 mmol) and Cs_2CO_3 (0.69 g, 2.1 mmol) were suspended in DMF (10 ml) and a solution of ethyl (2-bromoacetyl)glycinate (0.403 g, 1.8 mmol) in DMF (2 mL) was added dropwise. The mixture was stirred for 24 h and then the solvent was removed under vacuum. The crude product was purified by silica-gel chromatography (DCM:MeOH 95:5, $R_f = 0.25$) to obtain a pale yellow oil (0.21 g, 0.33 mmol, 46% yield). ^{1}H NMR (CD_3CN, 500 MHz): δ(ppm) = 1.21 (6H, t, CH_3CH_2O–), 3.02 (8H, m, –CH_2N), 3.18–3.24 (12H, m, –CH_2N, –CH_2NCH_2CO–), 3.75 (4H, m, –NCH_2Ph), 4.01 (4H, m, –CH_2NCH_2CO–), 4.12 (4H, q, CH_3CH_2O–), 7.38–7.43 (10H, m, –NCH_2Ph); ^{13}C NMR (CD_3CN, 125 MHz): δ(ppm) = 13.4 (CH_3CH_2O–), 41.3 (–$CONHCH_2CO$–), 47.7, 49.8, 50.5, 51.0 (CH_2N), 55.1 (–CH_2NCH_2CO–), 57.5 (–NCH_2Ph), 61.2 (CH_3CH_2O–), 129.0 (–Ph_{meta}), 129.2 (–Ph_{para}), 131.2 (–Ph_{ortho}), 137.7 (–Ph_{ipso}), 169.5 (–$CONHCH_2COOEt$), 170.1 (–$CONHCH_2COOEt$). ESI-MS (m/z): found 639.54 ($M+H^+$) (calc for $C_{34}H_{54}N_6O_6$:639.81).

Synthesis of 2,2′-(7,10-dibenzyl-1,4,7,10-tetraazacyclododecane-1,4-diyl) bis(acetylglycinamide) (DO2AMGly). The protected ligand (0.21 g, 0.33 mmol) was dissolved in an aqueous solution of LiOH (5 mL, 2 M) and methanol (5 mL), and the resulting solution was stirred for 4 h at 50 °C. The reaction mixture was brought to pH 5, concentrated in vacuo, and purified by semipreparative HPLC-MS with Method B. The final compound was obtained as a trifluoroacetic salt after lyophilization (0.13 g, 0.19 mmol, 57% yield). ^{1}H NMR (D_2O, 500 MHz): δ(ppm) = 2.66–2.95 (16H, m, –CH_2N), 3.13 (4H, m, –CH_2NCH_2CO–), 3.68–3.70 (8H, m, –NCH_2Ph, –CH_2NCH_2CO–), 7.23–7.26 (10H, m, –NCH_2Ph); ^{13}C NMR (D_2O, 125 MHz): δ(ppm) = 41.2 (–$CONHCH_2CO$–), 48.2–50.0 (CH_2N), 54.1 (–CH_2NCH_2CO–), 57.6 (–NCH_2Ph), 129.2 (–Ph_{para} and –Ph_{meta}), 131.0 (–Ph_{ortho}), 137.4 (–Ph_{ipso}), 173.3 (–$CONHCH_2COOEt$), 176.0 (–$CONHCH_2COOEt$). HPLC analysis (Method A): $t_r = 7.6$ min; ESI-MS (m/z): found 583.58 ($M+H^+$) (calc for $C_{30}H_{43}N_6O_6$:583.70).

Synthesis of MnDO2AMGly. DO2AMGly (10 mmol) was dissolved in water (1 mL), and the pH of the solution was adjusted to 6.5. A solution of $Mn(NO_3)_2$ was added stepwise to the former solution adjusting the pH to 6.5 after each addition. The longitudinal relaxation rate of water protons was measured after each addition (0.47 T, 298 K), and the data were plotted versus the total concentration of Mn(II) added. A linear dependence of the longitudinal relaxation rate was observed, which indicated the formation of the metal complex. The exact concentration of the Mn(II) ions in the solutions was measured via the bulk magnetic susceptibility (BMS) shift method (Mn(II) $\mu_{eff} = 5.94$ μB). MnDO2AMGly HPLC analysis (Method A): $t_r = 8.45$ min. ESI-MS (m/z): found 636.43 $(M+H)^+$ (calc for $C_{30}H_{41}MnN_6O_6$:636.62).

Relaxometric measurements. Proton relaxation measurements ($1/T_1$) and the resulting $1/T_1$ NMRD profiles were measured on a Fast-Field Cycling (FFC) Stelar SmarTracer Relaxometer over a continuum of magnetic field strengths from 0.00024 to 0.25 T (corresponding to 0.01-10 MHz proton Larmor Frequencies). The relaxometer operates under computer control with an absolute uncertainty in $1/T_1$ of ±1%. A precise control of the temperature was operated during the measurements by means of a Stelar VTC-91 airflow heater equipped with a calibrated copper constantan thermocouple (uncertainty of ±0.1 °C). Furthermore, the real temperature inside the probe head was additionally monitored by a Fluke 52 k/j digital thermometer (Fluke, Zürich, Switzerland). The manganeseconcentration was determined by measuring the bulk magnetic susceptibility shifts of the *t*-BuOH ^{1}H NMR signal. Additional data in the 20–128 MHz frequency range were obtained with a High Field Relaxometer (Stelar) equipped with the HTS-110 3T Metrology Cryogen-free Superconducting Magnet. The data were collected using the standard inversion recovery sequence (20 experiments, 2 scans) with a typical 90° pulse width of 3.5 ms and the reproducibility of the data was within ±0.5%.

Cytotoxicity assay. The viability and proliferation of J774 macrophagic cells were evaluated by methyl thiazolyl tetrazolium (MTT) assay. Typically, J774 cells were incubated in the culture medium (DMEM) at 37 °C in an atmosphere of 5% CO2 and 95% air for 24 h. Subsequently, the culture medium was removed. The cells were incubated in culture medium containing MnDO2AMGly with several increasing concentrations (0.1, 1, 10 and 100 μM) for another 24 h and washed with medium twice. 100 μL of the new culture medium containing MTT reagent (10%) was added to each well of the 96-well assay plate and incubated for 4 h to allow the formation of formazan dye. After removal of the medium, the purple formazan product was dissolved with DMSO for 15 min. Finally, the optical absorption of formazan was measured at 570 nm by iMARK microplate reader (Bio-Rad).

Mice. Six-week-old male C57BL/6 mice (n = 3) and BALB/C female mice (n = 4, Charles River Laboratories Italia S.r.l., Calco, Italia) were maintained under specific pathogen free conditions in the animal facility of the Molecular Biotechnology Center, University of Torino, and treated in accordance with the EU guidelines (EU2010/63). BALB/C mice were inoculated with 2.5×10^5 TS/A murine breast cancer cells in 100 μL of PBS on both flanks. All in vivo studies were conducted according to approved procedures of the Institutional Animal Care and Use Committee of the University of Torino.

MRI acquisitions. Mice were imaged with a 7T MRI Bruker Neo Avance (Bruker, Ettlingen, Germany) scanner with a 1H 30 mm quadrature body volume coil for biodistribution studies and with a 1T MRI Aspect M2 scanner (Aspect Magnet Technologies Ltd., Israel) equipped with a 1H 35 mm body volume coil for tumor imaging studies. Mice were anesthetized by injecting a mixture of tiletamine/zolazepam (Zoletil 100; Virbac, Milan, Italy) 20 mg/kg and xylazine (Rompun; Bayer, Milan, Italy) 5 mg/kg and placed supine and breath rate was monitored with an air pillow (SA Instruments, Stony Brook, NY, USA). Cannulation of the lateral tail vein with a 27G catheter was exploited for intravenous injection of the contrast agents.

Biodistribution studies. Six-week-old male C57BL/6 mice (n = 3) were administered with MnDO2AMGly at a dose of 0.03 mmol Mn/kg. T1-weighted images were acquired before and after i.v. injection at several time points: 0, 5 min, 15 min, 30 min, 1 h, 2 h, 4 h and 24 h. A T1-weighted multislice sequence was used with the following parameters: TR 300 ms; TE 5 ms; number of slices 16; slice thickness 1.5 mm; FOV 30 mm; matrix 192x192; eight averages; acquisition time 3 m 50 s. Region of interests (ROIs) were manually placed in several organs (liver, spleen, muscle, kidneys, heart and gallbladder) and signal intensity (SI) values were measured, and contrast enhancement calculated as (SIpost-SIpre)/SIpre×100.

Tumor imaging. Eight-week-old BALB/C male mice (n = 2 for MnDO2AMGly and n = 2 for Gadobenate dimeglumine (MultiHance, kindly provided by Bracco Imaging) were imaged with an Aspect 1T M2 system. After the scout image acquisition, a T2-weighted (T2w) anatomical image was acquired with a Fast Spin Echo sequence with the following parameters: TR 2500 ms; TE 44 ms; number of slices 10; slice thickness 1.5 mm; FOV 40 mm; matrix 152×160; four averages; acquisition time 3 m 20 s. A tail vein bolus injection of 0.1 mmol/kg MnDO2AMGly or of Multihance formulated at 50 mM in sterile water was administered, and the mouse was imaged with an axial T1-weighted (T1w) 3D spoiled Gradient Echo sequence at 2, 10, 40 min and 3 h post-injection with the following parameters:

TR 40 ms; TE 2.1 ms; Flip Angle: 60°: number of slices 8; slice thickness 1.5 mm; FOV 40 mm; matrix 128x128; acquisition time 58 s. ROIs were manually placed in muscle and tumors regions across multiple slices and signal intensity (SI) values were measured, normalized to the SI of the reference (a vial filled with a gadolinium solution) and contrast enhancement (CE) calculated as (SIpost-SIpre)/SIpre×100.

Statistical analysis. All statistical analysis was performed using GraphPad Prism 7. Comparisons of contrast enhancements in tumor and muscle regions between MnDO2AMGly and GdBOPTA at equal dose were made by a two-way Anova test with a Dunnet's post-hoc multiple correction test. For all correlations and comparisons, $P < 0.05$ was considered significant.

Acknowledgements

The Italian Ministry for Education and Research (MIUR) is gratefully acknowledged for yearly FOE funding to the Euro-BioImaging Multi-Modal Molecular Imaging Italian Node (MMMI). Open Access funding provided by Università degli Studi del Piemonte Orientale Amedeo Avogadro within the CRUI-CARE Agreement.

Conflict of Interest

The authors declare no conflict of interest.

Data Availability Statement

The data that support the findings of this study are available on request from the corresponding author. The data are not publicly available due to privacy or ethical restrictions.

Keywords: MRI · contrast agent · Manganese · relaxometry · tumor

[1] J. Wahsner, E. M. Gale, A. Rodríguez-Rodríguez, P. Caravan, *Chem. Rev.* **2019**, *119*, 957–1057.
[2] M. Botta, F. Carniato, D. Esteban-Gómez, C. Platas-Iglesias, L. Tei, *Future Med. Chem.* **2019**, *11*, 1461–1483.
[3] D. Pan, A. H. Schmieder, S. A. Wickline, G. M. Lanza, *Tetrahedron* **2011** *67*, 8431–8444.
[4] Z. Baranyai, F. Carniato, A. Nucera, D. Horvath, L. Tei, C. Platas-Iglesias, M. Botta, *Chem. Sci.* **2021**, *12*, 11138.
[5] E. M. Snyder, D. Asik, S. M. Abozeid, A. Burgio, G. Bateman, S. G. Turowski, J. A. Spernyak, J. R. Morrow, *Angew. Chem. Int. Ed.* **2020**, *59*, 2414–2419.
[6] J. M. Hazelton, M. K. Chiu, H. H. Abujudeh, *Curr. Radiol. Rep.* **2019**, *7*, 5.
[7] E. Lancelot, P. Desché, *Invest. Radiol.* **2020**, *55*, 20–24.
[8] F. K. Kalman, G. Tircso, *Inorg. Chem.* **2012**, *51*, 10065–10067.
[9] E. M. Gale, I. P. Atanasova, F. Blasi, I. Ay, P. Caravan, *J. Am. Chem. Soc.* **2015**, *137*, 15548–15557.
[10] E. M. Gale, H. Y. Wey, I. Ramsay, Y. F. Yen, D. E. Sosnovik, P. Caravan, *Radiology* **2018**, *286*, 865–872.
[11] D. J. Erstad, I. A. Ramsay, V. Clavijo Jordan, M. Sojoodi, B. C. Fuchs, K. K. Tanabe, P. Caravan, E. M. Gale, *Invest. Radiol.* **2019**, *54*, 697–703.
[12] Z. Garda, E. Molnár, N. Hamon, J. L. Barriada, D. Esteban Gómez, B. Váradi, V. Nagy, K. Pota, F. K. Kálmán, I. Tóth, N. Lihi, C. Platas-Iglesias, É. Tóth, R. Tripier, G. Tircsó, *Inorg. Chem.* **2021**, *60*, 1133–1148.
[13] M. Devreux, C. Henoumont, F. Dioury, S. Boutry, O. Vacher, L. V. Elst, M. Port, R. N. Muller, O. Sandre, S. Laurent, *Inorg. Chem.* **2021**, *60*, 3604–3619.
[14] F. K. Kalman, V. Nagy, B. Varadi, Z. Garda, E. Molnar, G. Trencsenyi, J. Kiss, S. Meme, W. Meme, E. Toth, G. Tircso *J. Med. Chem.* **2020**, *63*, 6057–6065.
[15] D. Ndiaye, M. Sy, A. Pallier, S. Même, I. de Silva, S. Lacerda, A. M. Nonat, L. J. Charbonnière, É. Tóth, *Angew. Chem. Int. Ed.* **2020**, *59*, 11958–11963; *Angew. Chem.* **2020**, *132*, 12056–12061.
[16] G. A. Rolla, C. Platas-Iglesias, M. Botta, L. Tei, L. Helm, *Inorg. Chem.* **2013**, *52*, 3268–3279.
[17] Z. Garda, A. Forgacs, Q. N. Do, F. K. Kalman, S. Timári, Z. Baranyai, L. Tei, I. Toth, Z. Kovacs, G. Tircso, *J. Inorg. Biochem.* **2016**, *163*, 206–213.
[18] G. A. Rolla, V. De Biasio, G. B. Giovenzana, M. Botta, L. Tei, *Dalton Trans.* **2018**, *47*, 10660–10670.
[19] G. Mulas, G. A. Rolla, C. F. G. C. Geraldes, L. W. E. Starmans, M. Botta, E. Terreno, L. Tei, *ACS Appl. Bio Mater.* **2020**, *3*, 2401–2409.
[20] A. Forgács, L. Tei, Z. Baranyai, I. Tóth, L. Zékány, M. Botta, *Eur. J. Inorg. Chem.* **2016**, 1165–1174.
[21] A. Forgács, L. Tei, Z. Baranyai, D. Esteban-Gómez, C. Platas-Iglesias, M. Botta, *Dalton Trans.* **2017**, *46*, 8494–8504.
[22] P. Foroozandeh, A. A. Aziz, *Nanoscale Res. Lett.* **2018**, *13*, 339.
[23] V. C. Pierre, M. Botta, S. Aime, K. N. Raymond, *Inorg. Chem.* **2006**, *45*, 8355–8364.
[24] D. L. Longo, F. Arena, L. Consolino, P. Minazzi, S. Geninatti-Crich, G. B. Giovenzana, S. Aime, *Biomaterials.* **2016**, *75*, 47–57.
[25] M. Botta, S. Avedano, G. B. Giovenzana, A. Lombardi, D.L Longo, C. Cassino, L. Tei, S. Aime, *Eur. J. Inorg. Chem.* **2011**, 802–810.
[26] J. Zhu, E. M. Gale, I. Atanasova, T. A. Rietz, P. Caravan, *Chem. Eur. J.* **2014**, *20*, 14507–14513.
[27] W. Cheng, T. Ganesh, F. Martinez, J. Lam, H. Yoon, R. B. Macgregor Jr., T. J. Scholl, H.-L. M. Cheng, X. Zhang, *J. Biol. Inorg. Chem.* **2014**, *19*, 229–235.
[28] S. Anbu, S. H. L. Hoffmann, F. Carniato, L. Kenning, T. W. Price, T. J. Prior, M. Botta, A. F. Martins, G. J. Stasiuk, *Angew. Chem. Int. Ed.* **2021**, *60*, 10736–10744.
[29] R. Kataki, D. Parker, A. Teasdale, J. P. Hutchinson, H. J. Buschmann, *J. Chem. Soc. Perkin Trans. 2* **1992**, *8*, 1347–1351.
[30] A. E. Merbach, L. Helm, E. Toth, *The Chemistry of Contrast Agents in Medical Magnetic Resonance Imaging*, Wiley, 2nd ed., **2013**.
[31] a) G. Lipari, S. Szabo, *J. Am. Chem. Soc.* **1982**, *104*, 4546; b) G. Lipari, S. Szabo, *J. Am. Chem. Soc.* **1982**, *104*, 4559.
[32] G. Fanali, Y. Cao, P. Ascenzi, M. Fasano, *J. Inorg. Biochem.* **2012**, *117*, 198–203.
[33] J. Zhu, E. M. Gale, I. Atanasova, T. A. Rietz, P. Caravan, *Chem. Eur. J.* **2014**, *20*, 14507–14513.
[34] K. Islam, S. Kim, H.-K. Kim, Y.-H. Kim, Y.-M. Lee, G. Choi, A. R. Baek, B. K. Sung, M. Kim, A. E. Cho, H. Kang, G.-H. Lee, S. H. Choi, T. Lee, J.-A. Park, Y. Chang, *Bioconjugate Chem.* **2018**, *29*, 3614–3625.
[35] A. Anemone, L. Consolino, D. L. Longo, *Eur. Radiol.* **2017**, *27*, 2170–2179.
[36] D. L. Longo, R. Stefania, C. Callari, F. De Rose, R. Rolle, L. Conti, L. Consolino, F. Arena, S. Aime, *Adv. Healthcare Mater.* **2017**, *6*, 1600550.
[37] S. Laurent, L. van der Elst, R. N. Muller, *Contrast Media Mol. Imaging* **2006**, *1*, 128–137.

Manuscript received: September 20, 2022
Revised manuscript received: October 5, 2022
Accepted manuscript online: October 5, 2022
Version of record online: October 27, 2022